Acta Materialia 241 (2022) 118362

Contents lists available at ScienceDirect

Acta Materialia

journal homepage: www.elsevier.com/locate/actamat

Pressureless flash sintering of α-SiC: Electrical characteristics and densification

Andrew Gibson[a], Yinsheng Li[a,b], Ruy Sebastian Bonilla[a], Richard I. Todd[a,*]

[a] Department of Materials, University of Oxford, Parks Road, Oxford OX1 3PH, UK
[b] Engineering Laboratory of Advanced Energy Materials, Ningbo Institute of Materials Technology and Engineering, Chinese Academy of Sciences, 1219 Zhongguan West Road, Ningbo, Zhejiang 315201, China

ARTICLE INFO

Article history:
Received 27 April 2022
Revised 16 August 2022
Accepted 12 September 2022
Available online 21 September 2022

Keywords:
Flash sintering
Silicon carbide
B and C sintering additives
Vickers hardness
Microstructure

ABSTRACT

The application of an electric field over a ceramic powder compact at elevated temperatures gives rise to "flash sintering". The phenomenon occurs at a critical combination of field and temperature, which leads to a rapid increase in the electric power dissipated within the sample. This results in sample densification in far shorter timescales than those required with conventional sintering. This paper reports the first successful pressureless flash sintering of SiC with B and C sintering aids. Mean relative densities of up to 94.4% have been achieved in several minutes using an alumina tube furnace at 1500 °C. The sample temperature during flash sintering was similar to those used for conventional sintering of SiC (2100–2200 °C). The electrical response of SiC during the flash event was consistent with thermal runaway. However, the negative temperature coefficient of resistivity responsible for the runaway originated primarily from the effects of sintering, in contrast to the case with oxide ceramics. The rapid sintering was attributed to the rapid heating and the formation of a liquid phase. The densest specimen had a grain size of 5.9 μm ± 0.5 μm and a Vickers hardness (HV5) of 24.7 GPa ± 0.5 GPa. These values were similar to those of conventionally sintered specimens of the same powder but the production time of the flash sintered samples was reduced by more than 6 h and with a furnace temperature lower by 700 °C.

1. Introduction

Flash sintering involves the heating of a powder compact whilst passing an electric current through it. Under investigation since it was reported in 2010 [1], it has now been successfully used to densify a wide range of ceramics [2–8]. The process is initiated by preheating specimens in a furnace and subjecting them to electric field strengths of 10–1000 V cm^{-1}. The preheating temperature is lower than conventional sintering temperatures and acts to reduce sample resistance, allowing electric current to flow. This causes resistive heating and a further rapid drop in sample resistance due to the negative temperature coefficient of resistance (NTC) characteristic of most ceramics. At constant voltage, this leads to thermal runaway, often termed the "flash event" [6], and this is subsequently controlled by limiting the current or power supplied to the sample. Sintering occurs during the process, usually at similar sample temperatures to those used in conventional heating but densification is achieved in a few seconds.

To date, the bulk of research on flash sintering has been conducted on oxide ceramics but the benefits of high speed and low furnace temperatures make flash sintering an attractive manufacturing method for non-oxide ceramics as well. These covalently bonded materials have important structural and functional uses including wear resistant and armour applications or as semiconductor power devices. However, production costs are typically very high due to the elevated temperatures and long densification times associated with traditional sintering techniques. Pressureless flash sintering of SiC using liquid phase, oxide sintering aids shows promise but the highest density achieved to date is 88% [6,9]. Low melting point sintering aids also compromise the high temperature properties of the SiC produced.

Higher densities have been achieved using B and C as sintering aids by flash spark plasma sintering (FSPS) [10,11]. However, specimens had to be pre-sintered by conventional SPS to give them sufficient strength to withstand the FSPS process and the attendant use of pressure requires expensive equipment and currently restricts the components produced to simple shapes such as plates [10,11]. FSPS has also been used to sinter ZrB_2 [12]. High flash sintered densities have also been achieved in WC without pre-sintering by applying a modest pressure (4 MPa) with the aid

* Corresponding author.
E-mail address: richard.todd@materials.ox.ac.uk (R.I. Todd).

https://doi.org/10.1016/j.actamat.2022.118362

of a non-conducting die [7,13]. Flash sintering of B_4C has been attempted, but sintering was only observed within localised hot spots and the bulk sample density did not increase from that of the green body [14].

The aim of the research reported in this paper was to achieve high densities by flash sintering of a non-oxide without the use of pressure for the first time. SiC with B and C sintering aids was used for good post-sintering temperature resistance. The novel apparatus and flash sintering methodology required for the successful manufacture of SiC through pressureless flash sintering is described. The flash sintering characteristics are compared with results from other materials reported in the literature.

2. Materials and methods

2.1. Sample preparation

All samples were made from H.C. Starck Starceram SQ premix, consisting of UF-15 α-SiC ($d_{50} \sim 0.75$ µm), sintering additives (2.5–3.5 wt% C, 0.5 wt% B), binder (PEG/PVA), supplied as spray dried $\sim$ 60 µm granules. The powder was uniaxially pressed into bars and cold isostatically pressed at 200 MPa. The green bodies had relative densities of ~60%. Typical dimensions of the volume of the green body between the flash sintering electrodes were: 22 × 6 × 2 mm.

2.2. Flash sintering apparatus

A modified alumina tube furnace with a windowed end provided the pre-heating to the samples. Holes were drilled at both ends of the sample, which were then threaded onto tungsten wires mounted on a removable flash sintering rig (Fig. S1 in Supplementary Material). Both ends of the sample and the areas of the sample directly around the electrodes were coated in PELCO© High Temperature Carbon Paste to reduce contact resistance. The whole rig was then sealed in the tube furnace. The current carrying wires protruded through one of the furnace end seals and were connected to the DC power supply (EA PS9750-60A-3W) for flash sintering. Data were recorded via a LabView script.

2.3. Flash sintering process

The furnace heating rate used in all experiments was 300 °C/h. To carbonise the binder, samples were first subjected to an isothermal hold at 800 °C in flowing N_2 (0.7 L/min) for 1 h before the furnace ramp continued to a designated furnace temperature. To ensure an inert sintering atmosphere, the gas supply was switched from N_2 to He 30 min before the electric field was applied across the sample (same flow rate). He suppressed the plasma formation upon application of the electric field, which occurred in some conditions when N_2 or Ar was used.

The electrical schedules investigated are split into two groups: constant voltage-constant power experiments with an increasing furnace temperature ramp (referred to below simply as constant voltage tests for brevity), and isothermal furnace temperature tests with a stepped power ramp (referred to as isothermal tests below).

During the former experiments, a constant voltage was initially applied across the sample in a furnace with gradually increasing temperature. Once the critical temperature was reached and runaway occurred, as described in Section 3.1, the furnace temperature was held constant. When the electrical power reached 400 W in these experiments, the power was maintained at this level. For consistency, the furnace temperature at which the power supply switched from voltage to power control was defined as the critical furnace temperature.

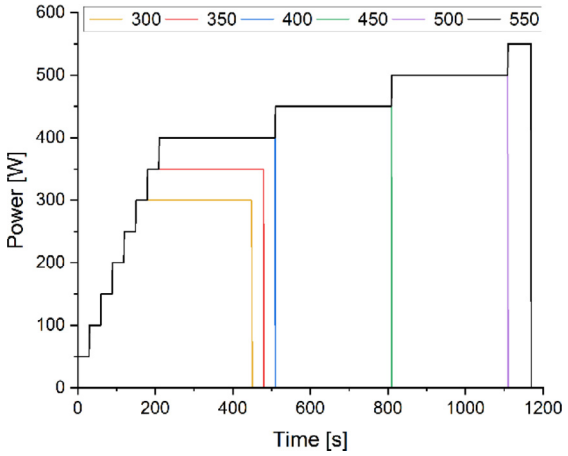

Fig. 1. Electrical power schedules in isothermal tests.

The isothermal experiments used a constant furnace temperature and the power was increased in a stepwise manner to the maximum power limit specific to that test. Fig. 1 shows a schematic of the power schedules investigated in this work. The maximum power limits investigated were 300 W, 350 W, 400 W, 450 W, 500 W and 550 W. The 300 W, 350 W and 400 W experiments all had an average ramp rate of 100 W/min and an isothermal power hold of 5 min. With this ramp rate and a furnace temperature of 1500 °C, the sample fractured above a power limit of 400 W. However, it was possible to extend the maximum limit to 550 W by reducing the electrical heating rate further. After 400 W, the rate was dropped to 10 W/min and ramped up to a maximum of 550 W for 1 min.

The effects of furnace temperature and hold time at the maximum power limit were investigated through variations of the stepped power heating schedules. For all these tests, an average power ramp of 100 W/min was used up to the maximum power limit. Maximum power limits of 460 W, 430 W and 400 W were used when investigating furnace temperatures of 1200 °C, 1350 °C and 1500 °C, respectively, to maintain similar sample temperatures between all tests. A hold time of 5 min at these power limits was used for all such experiments. Additional hold times were investigated (0.5, 5, 15 and 30 min) using a furnace temperature of 1500 °C and maximum power limit of 400 W.

2.4. Sample temperature estimation

The sample surface temperature was estimated using the black body radiation model [15]. The SiC emissivity was taken as 0.85 [16].

For the currents used in this investigation, a significant proportion of the electrical power was dissipated in the tungsten wires. To account for this, the energy loss in the wires was measured at the relevant currents and subtracted from the total power in the system to deduce the power dissipated in the specimen. Shrinkage was measured from video recordings. Both factors were accounted for when calculating sample temperatures and other quantities affected by them.

2.5. Conventional sintering

For comparison, conventionally sintered samples were produced based on the powder manufacturer's recommended sintering specifications. After the initial carbonisation described in Section 2.3, specimens were transferred to a graphite crucible and heated in Ar with a 300 °C/hr ramp to 2200 °C for a 2 h hold before ramping

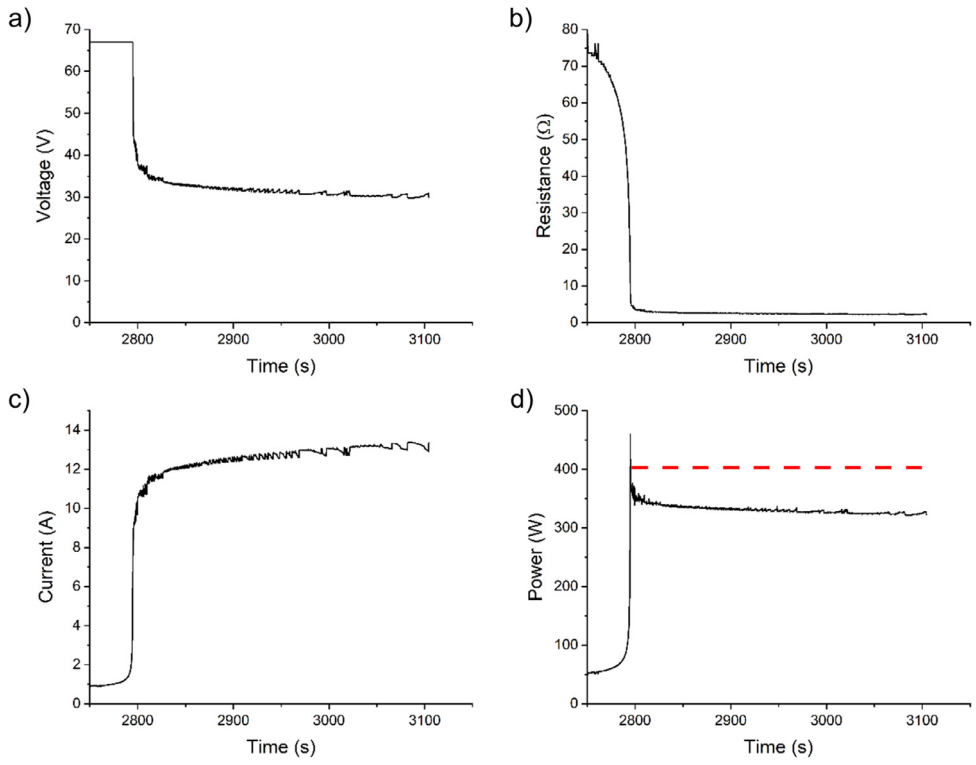

Fig. 2. The electrical response of a SiC specimen during a constant voltage (initial field 30 V cm^{-1}), furnace ramp experiment around runaway. (a) Voltage, (b) resistance, (c) current and (d) the power dissipated in the sample (total power including W wires represented by the dashed line). Sample temperature and other details are given for all constant voltage tests in Table 1.

down at the same rate. This temperature was chosen to be similar to the optimum temperature found for flash sintering. The sintering schedule is also within the powder manufacturer's recommended conditions of 2150 °C ± 50 °C with a 1–3 h dwell.

2.6. Specimen characterisation

The sample ends were removed and the resulting cuboids were sectioned on the plane midway between the electrodes. For each specimen half, a total of six density measurements were made using the Archimedes method, according to ASTM C380 -00 (2011). All densities are relative to the theoretical density (TD) of SiC: 3.21 g/cm^3. The central cross sections were polished with diamond suspensions down to 1 μm and finished with colloidal silica. Specimens were then chemically etched in Murakami's reagent (3 g potassium hydroxide, 30 g potassium ferricyanide and 60 g water) at 90 °C for 45 min.

Three equally spaced Vickers hardness indentations were made near the centre of the samples using a 5 kgf load. The samples were reground sufficiently to remove the first row of indents, polished and indents were made a second time for a total of six indents per specimen.

The microstructure was analysed and characterised using a Zeiss Merlin scanning electron microscope (SEM). Grain size estimations were made through the linear intercept method (using a multiplier of 1.56), using a minimum of 300 intercepts for each estimation. X-ray diffraction patterns (XRD) were collected using a Rigaku Miniflex Cu Kα diffractometer operated at 40 kV and 15 mA (0.01° step, 6 s $step^{-1}$).

The standard errors associated with density, grain size and hardness measurements were estimated from statistical distributions. Those associated with sample temperature, resistivity and critical field strength were estimated from the systematic and statistical errors associated with the electrical measurements, furnace temperatures, shrinkage from video recordings and the uncertainty in emissivity.

3. Results

3.1. Electrical response at constant voltage

Fig. 2 shows the electrical response from a sample during a constant voltage experiment with an initial electric field of 30 V cm^{-1}. Resistance decreased with time and consequently the current and therefore the dissipated power increased, slowly at first but increasing rapidly as the "flash event" [6] was approached, i.e. the hallmark electrical signature of flash sintering (~2790 s, Fig. 2). The furnace temperature at this flash point was 1032 °C ± 2 °C. Resistance dropped by a factor of ~25 compared with that of the green body immediately prior to the flash event. Once the power reached the predetermined limit of 400 W, the power supply moderated the voltage to maintain the total power at this level. The fall in sample power after the switch to power control in Fig. 2d is a consequence of the reduction in sample resistance, which leads to a higher proportion of the total power being dissipated in the wires.

Fig. 3 shows the effect of the electric field strength on power dissipated within specimens in the constant voltage tests. Lower electric field strengths required higher furnace temperatures to initiate flash sintering. The 15 V cm^{-1}specimens did not reach the flash event before the maximum furnace temperature of 1500 °C was reached. All other samples were held at a nominal power limit of 400 W for 5 min. Runaway occurred within ~60 s for field strengths of 35 V cm^{-1} and 40 V cm^{-1}. All other specimens displayed a maximum in power ("undulation") before the flash event. This is discussed in Section 4.2.

The results in Table 1 indicate that the higher furnace temperatures at the flash event for lower initial electric fields resulted in

Table 1
Furnace temperatures at runaway, sample temperatures during the isothermal hold stage and final specimen densities for varying initial electric field strengths in constant voltage experiments.

Electric field strength (V cm^{-1})	Furnace temp at runaway (°C)	Sample temp during hold (°C)	Density (%)
15	n/a	n/a	n/a
20	1364 ± 3	2085 ± 26	86.4 ± 0.5
25	1243 ± 2	2075 ± 26	81.5 ± 0.7
30	1032 ± 2	2020 ± 25	78.4 ± 0.7
35	820 ± 3	2010 ± 25	74.3 ± 1.3
40	802 ± 3	2005 ± 25	72.2 ± 0.8

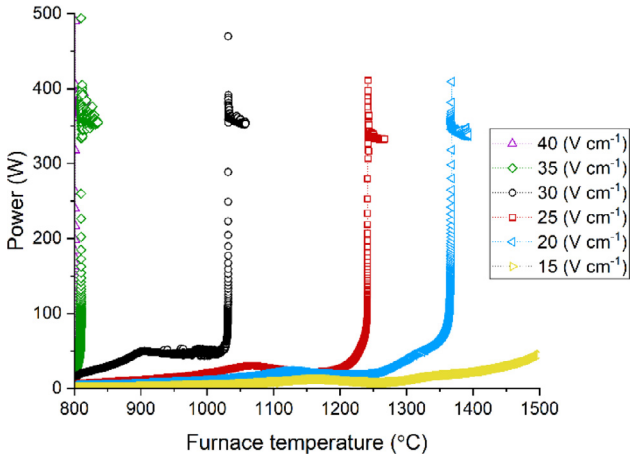

Fig. 3. Power dissipated in specimens against furnace temperature during constant initial electric field experiments, for varying electric field strengths.

higher sample temperatures and final sample densities. The highest density reached in this test series was 86.4% ± 0.5% by the 20 V cm^{-1} test with a sample temperature of 2085 °C ± 26 °C.

3.2. *Visual observations* in situ

Fig. S2 shows an image taken during an isothermal 400 W flash sintering experiment at a furnace temperature of 1500 °C. As with flash sintering of oxides, the ends of the specimen beyond the electrodes were much cooler than the electrically heated portion through which the majority of the current flowed, and the edges of the specimen were at a slightly lower temperature than the centreline. The heating was symmetrical with respect to the electrodes. In this case, the sample temperature was estimated to be ~ 2135 °C ± 27 °C based on the assumption of uniform surface temperature inherent in the black body model, and 90.3% ± 1.0% density was attained over a 5 min hold time. A video of this experiment is included in the Supplementary Material.

3.3. *Effect of flash sintering conditions in isothermal test results*

Fig. 4 shows how relative density varied with hold time and furnace temperature. The power followed the 400 W stepped heating schedule (Fig. 1). Longer sintering durations increased the density (Fig. 4a), although the effect of longer hold times reduced as higher densities were reached. The lowest recorded density was 84.8% ± 1.1% for a hold time of 0.5 min, which increased to 93.9% ± 0.6% for a 30 min hold time.

All samples in the furnace temperature tests (Fig. 4b) had similar sample temperatures (~2135 °C). Despite this, Fig. 4b indicates that sample density increased with furnace temperature, from 85.1% ± 1.2% at a furnace temperature of 1200 °C to 90.3% ± 1.0% at 1500 °C.

Fig. 5 shows the effect of maximum electrical power and resulting sample temperature on sample density for the power schedules in Fig. 1. Increasing the maximum power from 300 W to 400 W increased the relative density from 81.9% ± 0.6% to 90.3% ± 0.9%. Increasing sample temperatures beyond this power limit resulted in higher densities still, up to a maximum of 94.3% ± 0.4% with a specimen temperature of 2205 °C ± 28 °C. Exceeding 550 W or holding this limit for longer than 1 min resulted in sample fracture.

3.4. *Resistivity-temperature relationship*

From Fig. 6a, noticeable shrinkage begins at 180 s, at which point the specimen temperature is ~1975 °C. The majority of the shrinkage occurred before the power was ramped down, roughly 400 s after the onset of shrinkage. Fig. 6a indicates that a peak sample temperature of 2135 °C ± 27 °C was reached and a maximum isotropic shrinkage of 15% was achieved.

Fig. 6b shows the inverse Arrhenius plot for resistivity corresponding to the stepped power test in Fig. 6a. The electrical resistivity of the specimen decreased significantly as it was heated but there was little change during cooling. During heating, the resistivity of the sample continued to reduce during each constant power hold stage. Sample resistivity had reduced by a factor of ~18 by the end of the test compared with the specimen at the same temperature before the test.

3.5. *Microstructure and hardness*

The microstructure of a 94.4% ± 0.3% dense flash sintered SiC specimen is shown in Fig. 7. The micrographs show a mixture of equiaxed and elongated grains in the centre of the sample but fine and equiaxed grains at the edge. The central microstructure is markedly lower in porosity than the edge and has a larger grain size (5.9 μm ± 0.5 μm versus 1.8 μm ± 0.1 μm). The 2 mm length of the 6 × 2 mm cross section is denoted as the edge.

The hardness values of a 550 W isothermally flash sintered SiC specimen and SiC prepared by conventional sintering are shown in Table 2, along with density and average grain sizes from the centre of the cross sections. The grain size of the flash sintered specimen was slightly smaller and the mean density lower than that of the conventionally sintered specimen. The hardness values of the two materials were the same to within experimental uncertainty.

4. Discussion

4.1. *Phenomenology of the electrical response: the flash event at constant voltage*

Figs. 2 and 3 show that the electrical response of SiC leading up to the flash event at constant voltage was qualitatively similar to that of a wide variety of other ceramics [17]: a rapid drop in sample resistance occurred with a consequent increase in current

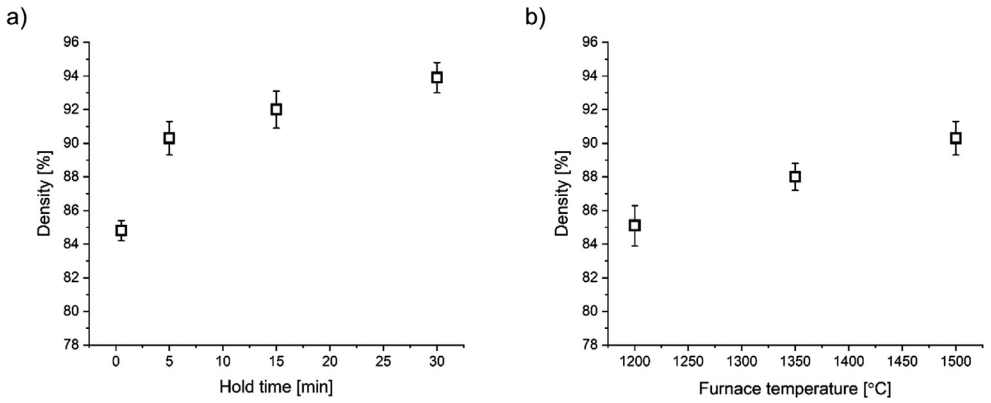

Fig. 4. Relative density against (a) hold time with a furnace temperature of 1500 °C and (b) furnace temperature for a hold time of 5 min and a constant specimen temperature of ~ 2135 °C.

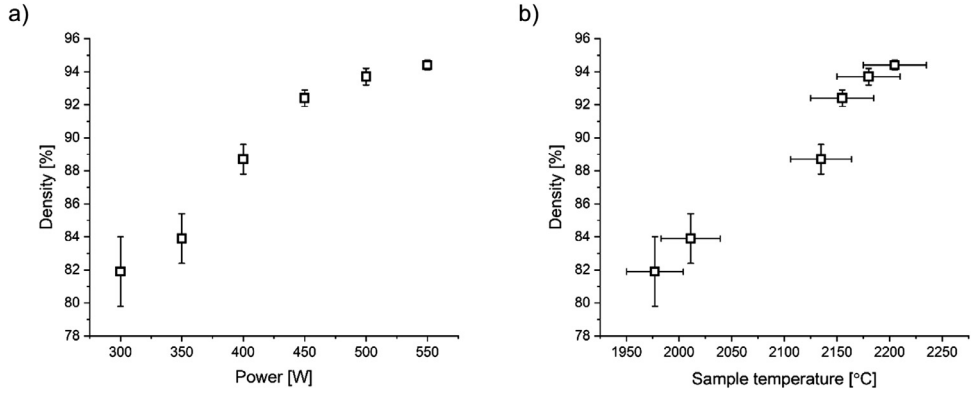

Fig. 5. Final sample density against (a) nominal maximum power and (b) maximum sample temperature for isothermal tests. The furnace temperature was 1500 °C.

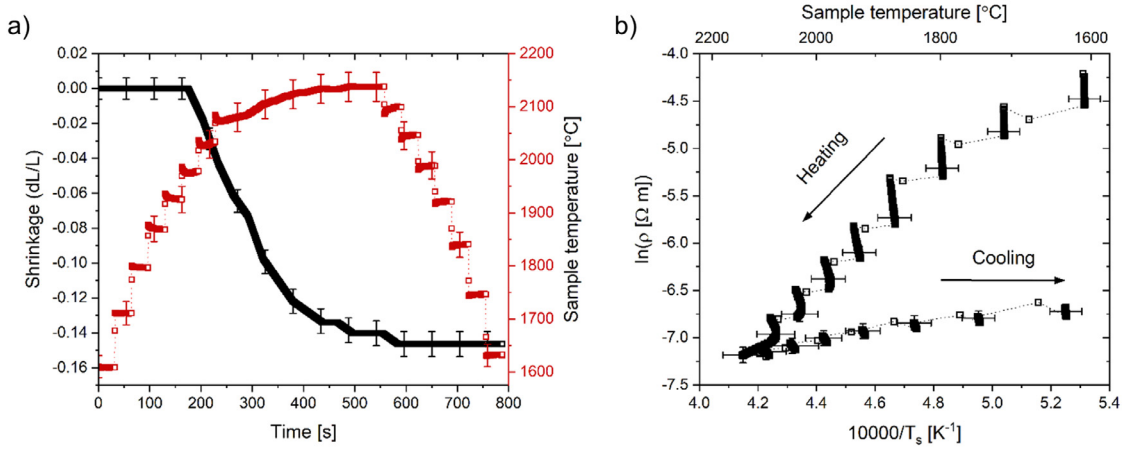

Fig. 6. (a) Specimen shrinkage (black) and sample temperature T_s (red) against time and (b) the corresponding inverse Arrhenius graph of resistivity during an isothermal test to a power limit of 400 W at a furnace temperature of 1500 °C. The sample was cooled at the same rate as it was heated. The effects of sample shrinkage and resistance in the wires were incorporated into the specimen resistivity and temperature calculations. For clarity, error bars are only included for a small proportion of data points.

Table 2
Mean density, Vickers hardness and grain size at the centre of the specimen for flash sintered and conventionally sintered SiC.

	Density (%)	HV5 (GPa)	Average grain size (μm)
550W Flash Sintered SiC	94.4 ± 0.3	24.7 ± 0.5	5.9 ± 0.5
Conventional SiC	97.0 ± 0.2	24.8 ± 0.5	10.2 ± 1.1

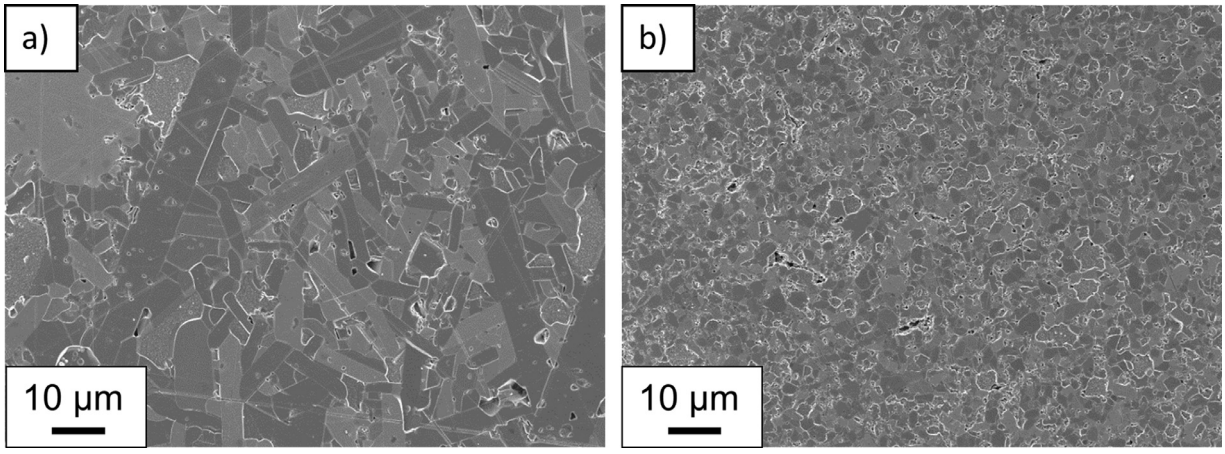

Fig. 7. SEM images at low and high magnification of the centre (a) and the edge (b) of the cross section of a SiC specimen flash sintering with a maximum power of 550 W and a constant furnace temperature of 1500 °C.

and electrical power dissipation. The reduction of the critical furnace temperature required for the flash event in SiC with increasing electric field (Fig. 3) is also typical behaviour.

Quantitative analysis of the electrical and thermal response of several oxides [18–22] during the flash event shows that it is caused by thermal runaway, in which the reduction of resistance as the sample temperature increases leads to a greater increase in power dissipation at constant voltage than can be lost from the sample surface as heat. The consequence is rapid electrical heating of the sample. The combination of electric field E and furnace temperature T_f at which runaway will occur is given by Todd et al. [19,23]:

$$E^2 = \frac{4p\varepsilon\sigma\rho_0 R}{AQ}\left(T_f + \Delta T_c\right)^5 \exp\left(\frac{Q}{R\left(T_f + \Delta T_c\right)}\right) \quad (1)$$

in which for $\Delta T_c \ll T_f$:

$$\Delta T_c \approx \frac{RT_f^2}{Q - 5RT_f} \quad (2)$$

In these equations, p and A are the perimeter and area of the specimen cross-section between the electrodes, ε the emissivity, σ Stefan's constant, ρ_0 the pre-exponential in the inverse Arrhenius expression for the resistivity as a function of temperature, R the gas constant, Q the activation energy for electrical resistivity/conductivity, and ΔT_c the excess temperature of the specimen relative to the furnace (i.e. $T_s - T_f$) at runaway. The equations can be used to predict the critical electric field for runaway at constant furnace temperature or the furnace temperature at which the flash event occurs during heating with a constant electric field. For materials whose conductivity deviates from Arrhenius behaviour, the effective values of Q and ρ_0 at the temperature of interest should be used.

The values of Q and ρ_0 for each of the three samples in Fig. 3 that exhibited flash events were deduced from the inverse Arrhenius plots for resistivity in Fig. 8a. The plots for all three specimens possess two approximately straight sections with a distinctive undulation in between. The flash event occurred at higher temperatures than the undulation so the values of Q and ρ_0 for each specimen were extracted using the straight sections immediately to the left of the undulations in Fig. 8(a) and are given in Table 3. The transition in behaviour will be discussed in the next section.

Fig. 8b compares the experimentally observed furnace temperatures at runaway for each initial electric field E with those predicted by solving Eqs. (1) and (2) for T_f using the values of Q and ρ_0 in Table 3 with $\varepsilon = 0.85$ [16] and the experimental values for p and A. The agreement is within experimental uncertainty, demonstrating that the "flash event" observed here in SiC was thermal runaway, as in oxide ceramics.

Table 3
Activation energies and pre-exponentials of resistivity for the data of Figs. 3 and 8(a) in the vicinity of the flash event.

Electric field strength (V cm^{-1})	Q (kJ mol^{-1})	ρ_0 (Ω m)
20	137	1.91×10^{-6}
25	127	3.94×10^{-6}
30	92	3.74×10^{-5}

4.2. Mechanisms influencing electric conductivity during flash sintering of SiC

The flash event at constant electric field analysed in the previous section originated in the NTC behaviour during heating evident in Figs. 6b and 8a. Most ceramic powder compacts exhibit NTC behaviour under the conditions of flash sintering. This can result from (i) the innate NTC behaviour of many ceramics caused by an increasing concentration or mobility of the charge carriers with temperature, (ii) extrinsic effects of the increase in current with temperature at constant voltage, such as the increasing component of electronic conductivity observed in YSZ under direct current as it becomes electrochemically reduced near the cathode [24], and (iii) the effect of the early stages of sintering in improving particle-particle contacts [23]. Electrochemical reduction is not expected to occur in an electronically conducting, covalently bonded semiconductor such as SiC, and the symmetrical appearance of the specimens during flash sintering (Fig. S2) suggests that any other effects of the direct current on resistivity were small. Fig. 6b also shows that the resistivity of the sintered specimen was almost constant during cooling between 2200 °C and 1500 °C, so the underlying NTC behaviour of the SiC itself is evidently also weak under these conditions. This temperature-independence of resistivity above 800 °C has also been reported for a range of α-SiC ceramics by Gnesin et al. [25]

The fall in resistivity during heating in Fig. 6b must therefore have been caused almost entirely by mechanisms associated with the sintering of the powder compact. This is demonstrated by the large difference in resistivity at $T_s \sim 1600$ °C in the heating and cooling parts of the cycle, and by the continuously decreasing resistivity at approximately constant specimen temperature during the constant power periods of the stepped profile used in the heat-

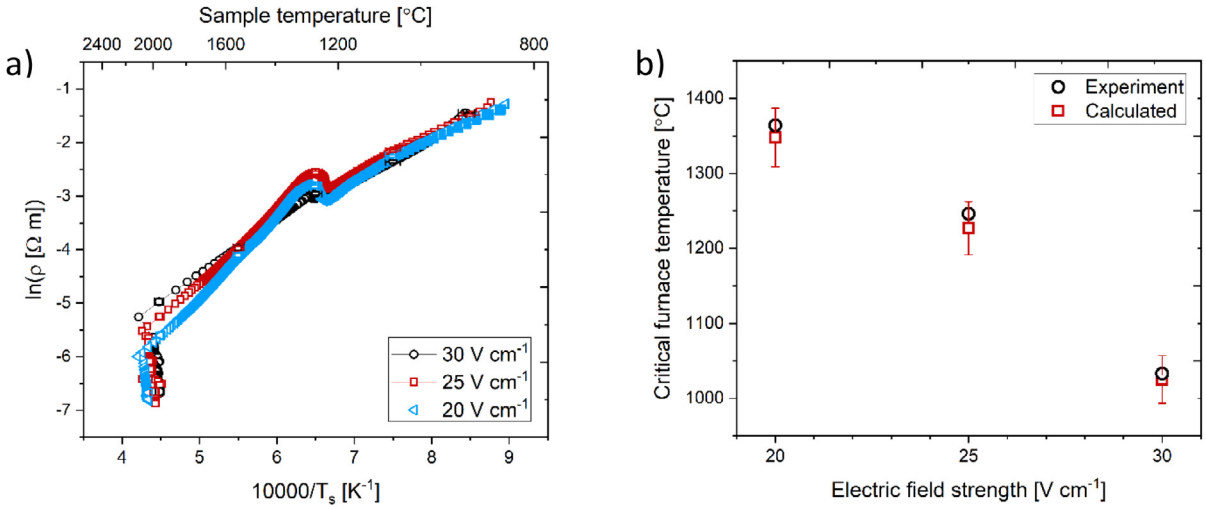

Fig. 8. (a) Data from the 30 V cm^{-1}, 25 V cm^{-1} and 20 V cm^{-1} constant initial electric field tests plotted as ln(ρ) vs 10000/T_s, where T_s is the specimen temperature and ρ the resistivity. For clarity, error bars are only shown for representative data points. (b) The predicted and observed critical furnace temperature against electric field strength.

ing portion of the cycle. Similar tests using pre-sintered specimens with pristine electrodes demonstrated that this reduction in resistance during heating cannot be attributed to an improvement of electrode contact (Fig. S3). The difference in resistivity before and after sintering in Fig. 6b corresponds to a factor of ~18. This is of the same order as the resistivity change measured before and after the flash sintering of 3YSZ [23] and is considered to be primarily the consequence of the improvement in the quality and area of connection between grains as sintering progresses. Analogous conclusions have been reached concerning the appearance of thermal runaway-driven flash events in WC and AA5083 aluminium alloy. The underlying resistivity of both of these materials increases with temperature (PTC behaviour) but their powder compacts initially exhibit NTC behaviour on the application of an electric field owing to the removal of oxides or other resistive contaminants from between the particles and the increase in contact area between the particles [13,26,27].

An additional contribution to the conductivity change during sintering from the diffusion of the boron sintering aid - an acceptor dopant - into the grains during sintering cannot be completely ruled out. The powder used for the current material is expected to be n-type owing to nitrogen doping from the atmosphere during production by the Acheson process [28]. The boron would be expected to counteract this [29,30], initially increasing the resistivity, although the relevant diffusion coefficients [31] suggest that the boron could only have diffused to the centre of the grains once the highest temperatures had been reached. Furthermore, even when holes become the charge carriers, boron additions are associated with an increase in the high temperature resistivity [25,32]. Given the strong reduction of resistivity during sintering shown in Fig. 8b, it is concluded that any such effect of boron is outweighed by the resistivity reduction caused by sintering described above.

The dependence of resistivity on sintering involves mainly indirect factors such as geometry, chemistry and thermal history that give no reason for an Arrhenius relationship to be obeyed. The straightness of the lines in Fig. 8a to the left of the undulations noted in the previous section is therefore coincidental. This also explains the variation of the values of activation energy Q in Table 3 with applied field E: these are *apparent* activation energies, not indicative of a particular transport mechanism and there is therefore no reason for them to be constant.

The distinctive undulations in Fig. 8a correspond to the transient peaks in power seen before the corresponding flash events in Fig. 3. These are suggested to be a consequence of the carbon sintering additives performing their role of removing the layer of silica present on the surface of the SiC powder particles. Estimated sample temperatures during this period were similar for all electric fields, at 1200 °C–1300 °C. The carbothermal [31] reduction of SiO_2 by C has been shown to take place in this temperature range [33,34]. It is suggested that the removal of the electrically insulating SiO_2 on the surfaces of the SiC grains initially increased the conductivity of the specimen. Eventually, the conductive free carbon was used up by the reaction with the SiO_2 and the specimen conductivity fell again, producing the peaks in Fig. 3. It is evident from Fig. 8a that the apparent activation energies are different before and after the undulation in each case, which is consistent with the proposed change in the chemistry of the conductive path through the specimen.

4.3. Densification and microstructural development

XRD showed that the main phases present in the flash sintered SiC were α-SiC polytypes (Fig. S4, Table S1). The sample temperature corresponding to the highest sintered density (2205 °C ± 28 °C, Fig. 5) is within the temperature range of 2150 °C ± 50 °C recommended by the manufacturer for conventional sintering of this powder and the main variables affecting conventional sintering had qualitatively similar effects in flash sintering. Thus, longer hold times and higher specimen temperatures tended to give higher densities (Figs. 4a and 5). However, the highest mean density achieved by flash sintering (94%) was lower than that of the conventionally sintered specimen (97%, Table 2). Magnani et al. [35] also reported a density of 97% by conventional sintering of the same powder.

The lower density achieved in flash sintering compared with conventional heating is attributable to the temperature gradients evident in Fig. S2, caused by heat loss at the surface of the specimen. This resulted in differential sintering, in which the hotter interior of the sample sintered faster than the colder, outer region (Fig. 7). For relatively low power levels, porosity remained in the cooler, exterior region of the sample when the interior of the sample was already dense. Conversely, noting that the flash sintering temperature estimations apply to the surface of the sample, if

the power was increased sufficiently to sinter the surface region of the specimen, the hotter interior may have started to decompose or to form excessive amounts of liquid phase on approaching the B_4C-SiC eutectic temperature of 2245 °C ± 5 °C [36,37]. This is the probable reason why specimen fracture prevented the further improvement of density by increasing the electrical power beyond 550 W. Thus, the achievable density was a compromise between densifying the outside of the specimen without degrading the central part.

The same problem of non-uniform temperature is also known in the flash sintering of YSZ and oxide liquid phase sintered SiC [6,9]. The effect was alleviated in this work by increasing the furnace temperature (Fig. 4b) and further improvements in density can be anticipated by the use of thermal insulation [38,39] around the specimen and by the use of more sophisticated electrode geometries [40] that concentrate the current towards the edge of the specimen.

The traditional view is that the main purpose of the C sintering additive is to remove SiO_2 at the surface of the SiC particles in order to raise the surface energy that drives sintering, whilst the B additive lowers the grain boundary energy, which opposes densification [41]. However, with sufficient B, a liquid phase can be formed at normal sintering temperatures, well below the B_4C-SiC eutectic temperature mentioned above [36,37]. Stobierksi and Gubernat [42] showed that this increases the rate of sintering and, above a certain level of B, can also cause the growth of abnormal, elongated grains such as those seen here in the centre of the specimens (Fig. 7). The SiC powder used in this work is the same as that used by Stobierski and Gubernat and the amounts of C and B are close to the maximum amount reported to give effective sintering without causing abnormal grain growth at 2150 °C. The nominal surface temperature of the specimens in Fig. 7 (2205 °C ± 28 °C) was slightly higher than this and the observation of elongated, abnormal grains, associated with liquid phase formation in the central part of the specimens in this work can be attributed to the even higher temperature experienced in the interior. Despite this, the average grain size at the centre of the flash sintered specimen was a little over half that of the conventionally sintered sample sintered at 2200 °C (Table 2). This is presumed to be a consequence of the much shorter hold times used for the flash sintered specimens.

By plunging the specimens into a ready-heated furnace, Stobierski and Gubernat were able to sinter green bodies with similar compositions to ours to ~92% dense in ~40 s at 2150 °C. Our flash sintered specimen with the same nominal temperature took 240 s to reach the same density and so, whilst also sintering very rapidly, was slightly slower than in the isothermal experiments of Stobierski and Gubernat. This demonstrates that, as with oxides such as YSZ [43] and ZnO [44], the electric field was not directly responsible for the rapid sintering and that the rapid heating was instead the main factor involved. Because of the requirement for stepped heating to avoid specimen fracture in this work, our heating rate was slower than that of Stobierski and Gubernat, which at least partly explains our slightly slower sintering rate. Nevertheless, manufacturing high density SiC with a small grain size in the order of minutes represents a considerable improvement on the powder manufacturer's recommendation of a 1–3 h dwell. In addition, the ability to sinter SiC in an alumina tube furnace at 1500 °C indicates that considerable savings in capital cost and energy consumption may be possible if the process is commercialised.

4.4. Vickers hardness

The Vickers hardnesses of the flash sintered and conventionally sintered SiC in this work were the same to within experimental error (24.7–24.8 GPa, Table 2). The values are higher than those reported by Wade et al. [45] for SiC of similar density using the same indentation load (approximately 22 GPa and 94% TD for coarse grained specimens and 23 GPa and 96% TD for fine grained specimens). It should be noted that the density of the central region tested in our material was higher than the mean value of 94%. Magnani et al. [35] measured a hardness of 23.4 GPa (10 kgf) for 97% dense samples made by pressureless sintering of the same powder as was used here. We conclude that the flash sintered SiC was at least as hard as pressurelessly sintered SiC.

5. Conclusions

SiC powder with B and C sintering additives has been successfully flash sintered without the use of pressure for the first time. A mean density of 94% TD was obtained in an alumina tube furnace at 1500 °C in 16 min. Most of the porosity in the specimen was near the edges of samples, where the temperature was lower. High sintered density was favoured by higher furnace temperatures, longer hold times and greater electrical power limits. The highest sintered density was obtained with a sample temperature during flash sintering of ~2200 °C. These high sample temperatures created a liquid phase during sintering that resulted in abnormal grain growth.

A "flash event", phenomenologically similar to those found in oxide ceramics, and characterised by a rapid rise in sample temperature followed by densification and accompanied by a decrease in sample resistivity, occurred under constant voltage conditions. A thermal runaway model based on the observed NTC behaviour of the resistivity during heating accurately predicted the conditions for the flash event. In contrast to oxide ceramics, however, the underlying electrical resistivity of the SiC had a weak temperature dependence in the temperature range of interest. The origin of the NTC behaviour and the thermal runaway was found to be the early stages of sintering, in which improved connectivity between the powder particles led to a reduction in resistivity.

The centre of the densest flash sintered SiC sample had an average grain size of 5.9 μm ± 0.5 μm and a Vickers hardness of 24.7 GPa ± 0.5 GPa. This hardness value was similar to that of a conventionally sintered specimen of the same powder. However, the average grain size of the flash sintered specimen was a little over half that of the conventionally sintered sample while the production time of the flash sintered sample was reduced by more than 6 h and with a furnace temperature lower by 700 °C.

Declaration of Competing Interest

The authors declare that they have no known competing financial interests or personal relationships that could have appeared to influence the work reported in this paper.

Acknowledgments

This work was supported by the Engineering and Physical Sciences Research Council (Grant number EP/R512060/1).

R. S. Bonilla was supported by the Royal Academy of Engineering under the Research Fellowship scheme.

The authors are grateful to Morgan Technical Ceramics for the conventional sintering of our powders.

Supplementary materials

Supplementary material associated with this article can be found, in the online version, at doi:10.1016/j.actamat.2022.118362.

References

[1] M. Cologna, B. Rashkova, R. Raj, Flash sintering of nanograin zirconia in <5 s at 850°C, J. Am. Ceram. Soc. 93 (2010) 3556–3559.
[2] M. Cologna, J.S.C. Francis, R Raj, Field assisted and flash sintering of alumina and its relationship to conductivity and MgO-doping, J. Eur. Ceram. Soc. 31 (2011) 2827–2837.
[3] A. Karakuscu, et al., Defect structure of flash-sintered strontium titanate, J. Am. Ceram. Soc. 95 (2012) 2531–2536.
[4] A.L.G. Prette, M. Cologna, V. Sglavo, R. Raj, Flash-sintering of Co2MnO4 spinel for solid oxide fuel cell applications, J. Power Sources 196 (2011) 2061–2065.
[5] R. Muccillo, E.N.S. Muccillo, M Kleitz, Densification and enhancement of the grain boundary conductivity of gadolinium-doped barium cerate by ultra fast flash grain welding, J. Eur. Ceram. Soc. 32 (2012) 2311–2316.
[6] E. Zapata-Solvas, S. Bonilla, P.R. Wilshaw, R.I Todd, Preliminary investigation of flash sintering of SiC, J. Eur. Ceram. Soc. 33 (2013) 2811–2816.
[7] I. Mazo, A. Molinari, V.M Sglavo, Effect of pressure on the electrical resistance flash sintering of tungsten carbide, J. Eur. Ceram. Soc. 42 (2022) 2028–2038.
[8] C. Schmerbauch, J. Gonzalez-Julian, R. Röder, C. Ronning, O Guillon, Flash sintering of nanocrystalline zinc oxide and its influence on microstructure and defect formation, J. Am. Ceram. Soc. 97 (2014) 1728–1735.
[9] V.M. Candelario, R. Moreno, R.I. Todd, A.L Ortiz, Liquid-phase assisted flash sintering of SiC from powder mixtures prepared by aqueous colloidal processing, J. Eur. Ceram. Soc. 37 (2017) 485–498.
[10] S. Grasso, et al., Flash Spark Plasma Sintering (FSPS) of α and β SiC, J. Am. Ceram. Soc. 99 (2016) 1534–1543.
[11] E.A. Olevsky, S.M. Rolfing, A.L Maximenko, Flash (ultra-rapid) spark-plasma sintering of silicon carbide, Sci. Rep. 6 (2016) 33408.
[12] S. Grasso, et al., Flash spark plasma sintering (FSPS) of pure ZrB2, J. Am. Ceram. Soc. 97 (2014) 2405–2408.
[13] I. Mazo, A. Molinari, V.M Sglavo, Electrical resistance flash sintering of tungsten carbide, Mater. Des. 213 (2022) 110330.
[14] A. Rosenberger, R.E. Brennan, A.L Fry, Flash sintering feasibility study and localized densification in boron carbide, J. Am. Ceram. Soc. 104 (2021) 3823–3827.
[15] R. Raj, Joule heating during flash-sintering, J. Eur. Ceram. Soc. 32 (2012) 2293–2301.
[16] M. Balat-Pichelin, A. Bousquet, Total hemispherical emissivity of sintered SiC up to 1850 K in high vacuum and in air at different pressures, J. Eur. Ceram. Soc. 38 (2018) 3447–3456.
[17] M. Biesuz, V.M Sglavo, Flash sintering of ceramics, J. Eur. Ceram. Soc. 39 (2019) 115–143.
[18] Y. Zhang, J.Il Jung, J Luo, Thermal runaway, flash sintering and asymmetrical microstructural development of ZnO and ZnO-Bi_2O_3 under direct currents, Acta Mater. 94 (2015) 87–100.
[19] R.I. Todd, E. Zapata-Solvas, R.S. Bonilla, T. Sneddon, P.R. Wilshaw, Electrical characteristics of flash sintering: thermal runaway of Joule heating, J. Eur. Ceram. Soc. 35 (2015) 1865–1877.
[20] M. Biesuz, V.M. Sglavo, Flash sintering of alumina: Effect of different operating conditions on densification, J. Eur. Ceram. Soc. 36 (2016) 2535–2542.
[21] E. Bichaud, J.M. Chaix, C. Carry, M. Kleitz, M.C. Steil, Flash sintering incubation in Al_2O_3/TZP composites, J. Eur. Ceram. Soc. 35 (2015) 2587–2592.
[22] J.G.P. da Silva, H.A. Al-Qureshi, F. Keil, R Janssen, A dynamic bifurcation criterion for thermal runaway during the flash sintering of ceramics, J. Eur. Ceram. Soc. 36 (2016) 1261–1267.
[23] M. Yoshida, S. Falco, R.I. Todd, Measurement and modelling of electrical resistivity by four-terminal method during flash sintering of 3YSZ, J. Ceram. Soc. Jpn. 126 (2018) 579–590.
[24] M. Biesuz, et al., Investigation of electrochemical, optical and thermal effects during flash sintering of 8YSZ, Materials (Basel) 11 (2018) 1214.
[25] G.G. Gnesin, V.K. Zakharenkov, L.A Shipilova, Volume electrical resistivity of silicon carbide heating elements, Sov. Powder Metall. Met. Ceram. 17 (1978) 72–76.
[26] B. McWilliams, J. Yu, F. Kellogg, S Kilczewski, Enhanced sintering kinetics in aluminum alloy powder consolidated using DC electric fields, Metall. Mater. Trans. A Phys. Metall. Mater. Sci. 48 (2017) 919–929.
[27] B. McWilliams, J. Yu, F Kellogg, Sintering aluminum alloy powder using direct current electric fields at room temperature in seconds, J. Mater. Sci. 53 (2018) 9297–9304.
[28] Y. Takeda, K. Nakamura, K. Maeda, Y Matsushita, Effects of elemental additives on electrical resistivity of silicon carbide ceramics, J. Am. Ceram. Soc. 70 (1987) 266–267.
[29] Y. Li, et al., Microstructure, thermal conductivity, and electrical properties of *in situ* pressureless densified SiC-BN composites, J. Am. Ceram. Soc. 98 (2015) 879–887.
[30] Y. Li, et al., High electrical resistivity of pressureless sintered *in situ* SiC-BN composites, Scr. Mater. 69 (2013) 740–743.
[31] N. Mokhov, E, Doping of SiC crystals during sublimation growth and diffusion, Cryst. Growth (2019), doi:10.5772/intechopen.82346.
[32] V.L. Kuznetsova, R.I. Bresker, Effect of B4C additions on the electric resistance of silicon carbide heaters, Refractories 13 (1972) 334–335.
[33] P.D. Miller, J.G. Lee, I.B Cutler, The reduction of silica with carbon and silicon carbide, J. Am. Ceram. Soc. 62 (1979) 147–149.
[34] W.J. Clegg, Role of carbon in the sintering of boron-doped silicon carbide, J. Am. Ceram. Soc. 83 (2000) 1039–1043.
[35] G. Magnani, A. Brentari, E. Burresi, G Raiteri, Pressureless sintered silicon carbide with enhanced mechanical properties obtained by the two-step sintering method, Ceram. Int. 40 (2014) 1759–1763.
[36] P.T.B. Shaffer, The SiC phase in the system SiC-B4C-C, Mater. Res. Bull. 4 (1969) 213–219.
[37] M. Asadikiya, C. Rudolf, C. Zhang, B. Boesl, Y. Zhong, The role of calphad approach in the sintering of B4C with SIC as a sintering aid by spark plasma sintering technique, Addit. Manuf. Strateg. Technol. Adv. Ceram. 258 (2016) 185–191.
[38] M. Biesuz, et al., Thermally-insulated flash sintering, Scr. Mater. 162 (2019) 99–102.
[39] A.G. Storion, et al., Effect of thermal insulation on microstructural homogeneity and onset temperature of flash sintered materials, J. Eur. Ceram. Soc. 41 (2021) 7807–7815.
[40] Y. Li, et al., Promoting core/surface homogeneity during flash sintering of 3YSZ ceramic by current path management: experimental and modelling studies, J. Eur. Ceram. Soc. 41 (2021) 6649–6659.
[41] H. Tanaka, Silicon carbide powder and sintered materials, Journal of the Ceramic Society of Japan 119 (1387) (2011) 218–233.
[42] L Stobierski, A Gubernat, Sintering of silicon carbide II. Effect of boron, Ceram. Int. 29 (4) (2003) 355–361.
[43] W. Ji, et al., Ultra-fast firing: effect of heating rate on sintering of 3YSZ, with and without an electric field, J. Eur. Ceram. Soc. 37 (2017) 2547–2551.
[44] Y. Zhang, J. Nie, J.M. Chan, J Luo, Probing the densification mechanisms during flash sintering of ZnO, Acta Mater. 125 (2017) 465–475.
[45] J. Wade, S. Ghosh, P. Claydon, H Wu, Contact damage of silicon carbide ceramics with different grain structures measured by Hertzian and Vickers indentation, J. Eur. Ceram. Soc. 35 (2015) 1725–1736.